Electronic Supporting Information

for

One-pot Route to X-Perfluoroarenes (X = Br, I) Based on Fe^{III}-assisted C–F Functionalization and Utilization of These Arenes as Building Blocks for Crystal Engineering Involving Halogen Bonding

Anton V. Rozhkov,[1] Anastasiya A. Eliseeva,[1] Sergey V. Baykov,[1] Bartomeu Galmés,[2]

Antonio Frontera,*[2] Vadim Yu. Kukushkin*[1,3]

[1]*Institute of Chemistry, Saint Petersburg State University, Universitetskaya Nab. 7/9,*

Saint Petersburg, 199034, Russian Federation

[2]*Deparment of Chemistry, Universitat de les Illes Balears, Crts de Valldemossa km. 7.5,*

07122 Palma de Mallorca (Baleares), SPAIN.

[3]*Laboratory of Crystal Engineering of Functional Materials, South Ural State University, 76,*

Lenin Av., Chelyabinsk, 454080, Russian Federation

S1. X-ray diffraction and theoretical studies

S1.1 Crystal data and structure refinement

Table S1. Crystal data and structure refinement for **3**–**4**, **7**.

	3	**4**	**7**
CCDC No.	1999374	1999377	1999379
Empirical formula	$C_{12}F_9I$	$BrC_{12}F_9$	$C_{12}F_8I_2$
M_W/g	442.02	395.03	549.92
T/K	100(2)	100(2)	100(2)
Radiation	Mo$K\alpha$ (λ = 0.71073)	Mo$K\alpha$ (λ = 0.71073)	Mo$K\alpha$ (λ = 0.71073)
Crystal color, shape	clear colorless, octahedral	colorless, octahedral	colorless, prism
Crystal size/mm^3	0.84 × 0.62 × 0.35	0.46 × 0.28 × 0.18	0.30 × 0.17 × 0.10
Crystal system	monoclinic	monoclinic	orthorhombic
Space group	C2/c	C2/c	Pbcn
a/Å	21.1443(11)	20.8814(10)	14.8168(18)
b/Å	8.0974(4)	8.0219(3)	10.3805(15)
c/Å	14.2425(6)	13.6868(7)	8.6880(11)
α/°	90	90	90
β/°	97.186(5)	97.136(5)	90
γ/°	90	90	90
V/Å^3	2419.4(2)	2274.90(18)	1336.3(3)
Z	8	8	4
ρ_c/g·cm^{-3}	2.427	2.307	2.733
μ/mm^{-1}	2.755	3.728	4.792
F(000)	1648.0	1504.0	1000.0
2Θ range/°	5.766 to 62.332	5.446 to 64.514	6.706 to 54.99
Reflections collected	6791	12969	6330
Independent reflections	3428 [R_{int} = 0.0237, R_{sigma} = 0.0371]	3658 [R_{int} = 0.0335, R_{sigma} = 0.0339]	1535 [R_{int} = 0.0335, R_{sigma} = 0.0261]
Data/restraints/parameters	3428/0/200	3658/0/199	1535/0/100
Goodness-of-fit on F^2	1.088	1.076	1.110
Final R indexes [$I \geq 2\sigma(I)$]	R_1 = 0.0272, wR_2 = 0.0583	R_1 = 0.0496, wR_2 = 0.1326	R_1 = 0.0250, wR_2 = 0.0592
Final R indexes [all data]	R_1 = 0.0325, wR_2 = 0.0583	R_1 = 0.0631, wR_2 = 0.1410	R_1 = 0.0330, wR_2 = 0.0653
Largest diff. peak/hole / e·Å^{-3}	0.88/-0.78	1.27/-1.06	0.75/-0.84

Table S2. Crystal data and structure refinement for the adducts.

	1·½[Ph_3PBn]I	**2**·[*n*-Bu_4N]I	**3**·[*n*-Bu_4N]I	**6**·[*n*-Bu_4N]I	**7**·[*n*-Bu_4N]I
CCDC No.	1999386	1999387	1999389	1999390	1999393
Empirical formula	$C_{37}H_{22}F_{10}I_3P$	$C_{22}H_{36}BrF_5IN$	$C_{28}H_{36}F_9I_2N$	$C_{26}H_{36}BrF_7IN$	$C_{28}H_{36}F_8I_3N$
M_W/g	1068.21	616.33	811.38	702.37	919.28
T/K	100(2)	100(2)	100(2)	100(2)	100(2)
Radiation	CuKα (λ = 1.54184)	Mo*Kα* (λ = 0.71073)	CuKα (λ = 1.54184)	CuKα (λ = 1.54184)	CuKα (λ = 1.54184)
Crystal color, shape	colorless, prism	colorless, plate	colorless, prism	colorless, prism	clear colorless, prism
Crystal size/mm^3	0.283 × 0.099 × 0.026	0.18 × 0.14 × 0.05	0.36 × 0.17 × 0.10	0.35 × 0.18 × 0.10	0.2 × 0.15 × 0.15
Crystal system	triclinic	monoclinic	monoclinic	monoclinic	triclinic
Space group	P-1	$P2_1/c$	$P2_1/c$	$P2_1/c$	P-1
a/Å	10.2393(8)	24.0165(12)	28.0093(4)	26.0491(2)	11.9736(7)
b/Å	13.6558(6)	7.7405(3)	8.01206(12)	7.89570(10)	12.1384(7)
c/Å	14.2346(9)	14.1780(6)	14.19750(17)	14.01250(10)	12.5839(6)
α/°	74.294(5)	90	90	90	88.791(4)
β/°	71.458(6)	95.897(4)	97.3595(11)	99.9450(10)	86.919(4)
γ/°	87.706(5)	90	90	90	63.430(6)
V/$Å^3$	1814.3(2)	2621.7(2)	3159.85(7)	2838.73(5)	1633.41(16)
Z	2	4	4	4	2
ρ_c/g·cm^{-3}	1.955	1.561	1.706	1.643	1.869
μ/mm^{-1}	21.419	2.789	16.279	11.064	23.117
F(000)	1016.0	1232.0	1592.0	1400.0	884.0
2*Θ* range/°	6.732 to 139.984	5.116 to 69.612	3.18 to 145.67	3.444 to 140.962	7.034 to 153.018
Reflections collected	24760	22276	18273	24386	31463
Independent reflections	6682 [R_{int} = 0.0772, R_{sigma} = 0.0608]	10511 [R_{int} = 0.0295, R_{sigma} = 0.0460]	6246 [R_{int} = 0.0448, R_{sigma} = 0.0428]	5437 [R_{int} = 0.0449, R_{sigma} = 0.0336]	6725 [R_{int} = 0.0535, R_{sigma} = 0.0308]
Data/restraints/parameters	6682/0/460	10511/0/275	6246/0/365	5437/0/329	6725/4/388
Goodness-of-fit on F^2	1.102	1.028	1.044	1.058	1.040
Final *R* indexes [$I \geq 2\sigma(I)$]	R_1 = 0.0510, wR_2 = 0.1383	R_1 = 0.0351, wR_2 = 0.0576	R_1 = 0.0365, wR_2 = 0.0985	R_1 = 0.0242, wR_2 = 0.0592	R_1 = 0.0371, wR_2 = 0.0949
Final *R* indexes [all data]	R_1 = 0.0542, wR_2 = 0.1418	R_1 = 0.0545, wR_2 = 0.0632	R_1 = 0.0409, wR_2 = 0.1025	R_1 = 0.0263, wR_2 = 0.0605	R_1 = 0.0432, wR_2 = 0.1001
Largest diff. peak/hole / *e*·$Å^{-3}$	2.30/-1.52	1.01/-0.67	0.97/-0.97	0.58/-0.38	1.35/-1.82

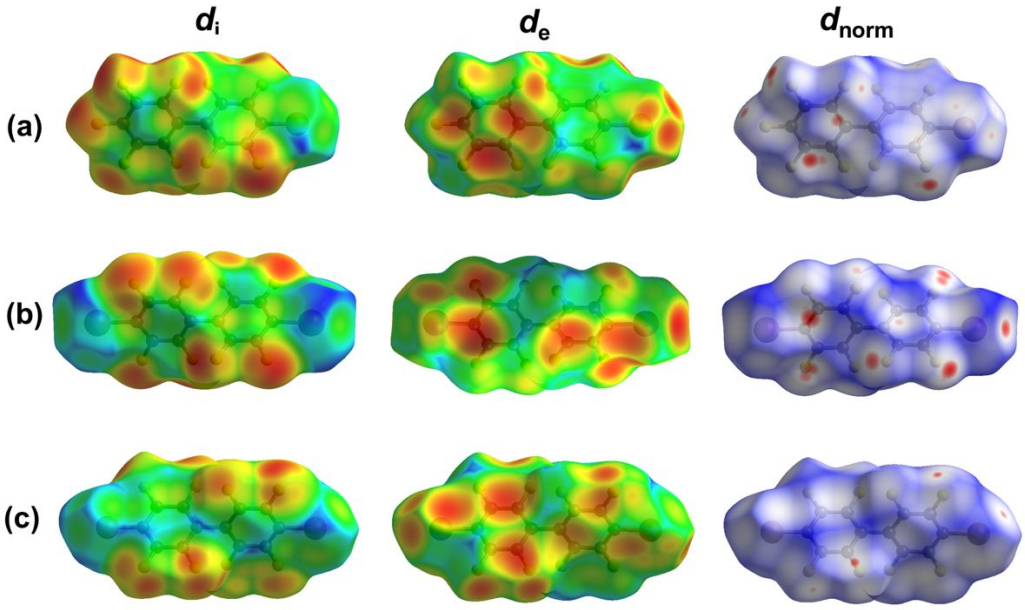

Fig. S1. Hirshfeld surfaces for the XRD structures of **4** (*a*) and **7**–**8** (*b*–*c*): d_i is the distance from the surface to the nearest nucleus internal to the surface, normalized by R_{vdW} of the involving atoms; d_e is the distance from the surface to the nearest nucleus external to the surface, normalized by R_{vdW} of the involving atoms; d_{norm} is a normalized contact distance obtained as the sum of d_i and d_e quantities, where intermolecular contacts closer than ΣR_{vdW} highlighted in red, longer contacts are blue, and contacts around ΣR_{vdW} are white.

Table S3. Results of HSA for the XRD structures of **3**–**4** and **7**–**8**.

XRD structure	Contributions of different intermolecular contacts to the molecular Hirshfeld surface*
3	F–F 49.3%, C–F 22.8%, I–F 17.6%, C–I 6.5%, C–C 3.6%
4	F–F 50.1%, C–F 24.0%, Br–F 16.2%, C–Br 5.5%, C–C 4.2%
7	I–F 40.3%, C–F 31.3%, F–F 22.1%, C–I 3.6%, I–I 2.7%
8	F–F 35.7%, Br–F 27.3%, C–F 21.4%, C–Br 8.5%, Br–Br 4.3%, C–C 2.8%

*The contributions of all other intermolecular contacts do not exceed 1%.

Table S4. Parameters of C–X···F (X = Br, I) XBs in **3**–**4** and **7**–**8**.

Structure	Contact	*d*(X···F), Å	∠(C–X···F),°	∠(C–F···X),°	R[a]
3	C4–I1···F9–C12	3.4287(15)	150.68(7)	137.94(13)	0.99
4	C4–Br1···F9–C12	3.305(2)	153.34(10)	138.35(18)	1.00
7	C4–I1···F4–C6	3.2813(19)	146.65(10)	135.49(16)	0.95
8	C4–Br1···F5–C8	3.2520(18)	149.09(12)	132.74(15)	0.98
	Comparison[b]		*150<∠<180*	*90*	

[a] R is a ratio between the interatomic distance and ΣR_{vdW}; ΣR_{vdW} are: $R_{vdW}(I) + R_{vdW}(F) = 3.45$ Å, $R_{vdW}(Br) + R_{vdW}(F) = 3.32$ Å.
[b] Comparison with the typical XB angles.

Table S5. Parameters of C···X–C (X = F, Br, I) LP–π short contacts in **3**–**4** and **7**–**8**.

Structure	Contact	*d*(C···F), Å	∠(C···F–C),°	R[a]
3	C5···I1–C4[b]	3.651(2)	77.10(7)	0.99
	C6···I1–C4[b]	3.679(2)	98.85(7)	1.00
4	C5···Br1–C4[b]	3.495(3)	76.88(11)	0.98
	C6···Br1–C4[b]	3.515(3)	99.69(11)	0.99
7	C3···F3–C5	2.956(4)	155.24(19)	0.93
8	C5···Br1–C4	3.598(4)	83.41(10)	1.01

[a] R is a ratio between the interatomic distance and ΣR_{vdW}; ΣR_{vdW} are: $R_{vdW}(C) + R_{vdW}(I) = 3.68$ Å, $R_{vdW}(C) + R_{vdW}(Br) = 3.55$ Å, $R_{vdW}(C) + R_{vdW}(F) = 3.17$ Å.
[b] 'From-the-bond' (C–C)···X–C (X = Br, I) LP–π contacts.

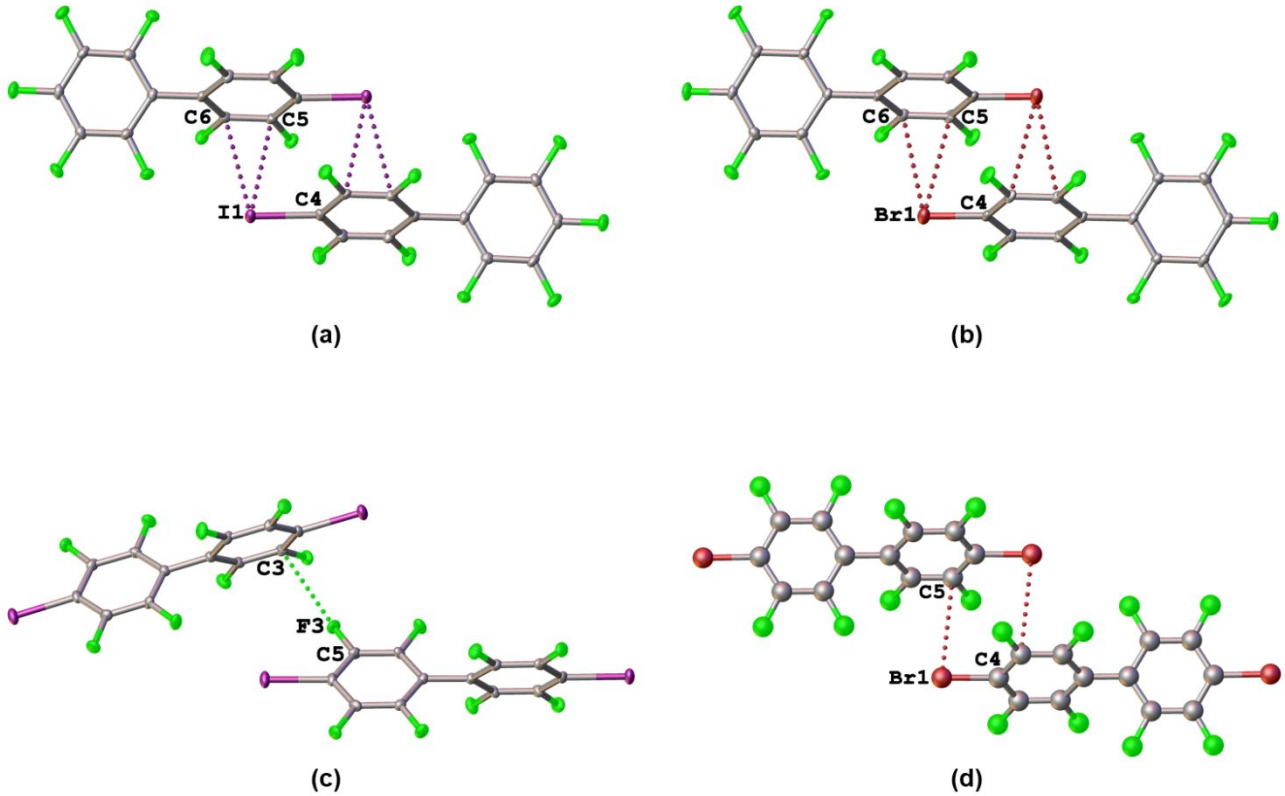

Fig. S2. The C···X–C (X = F, Br, I) LP–π short contacts in the crystal structures of **3** (*a*), **4** (*b*), **7** (*c*), and **8** (*d*). Thermal ellipsoids are shown with the 50% probability.

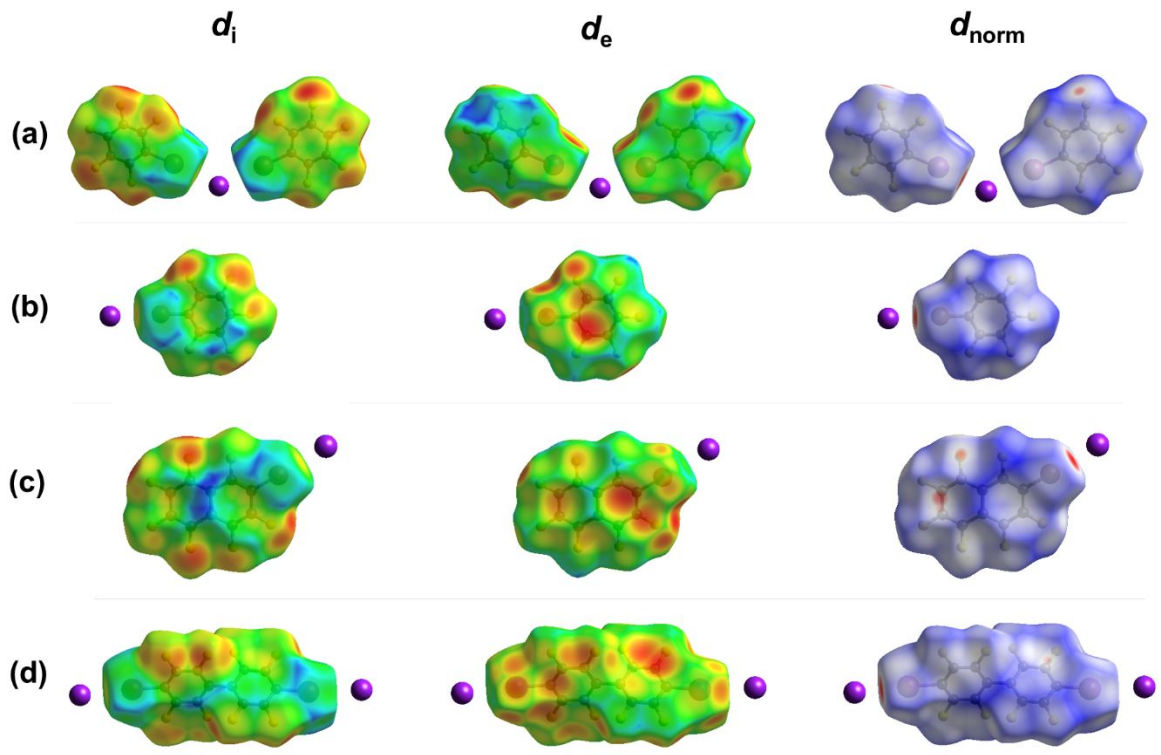

Fig. S3. Hirshfeld surfaces for **1** (*a*), **2** (*b*), **6** (*c*), and **7** (*d*) in the XRD structures of the obtained adducts. The remaining figure legend is as on **Fig. S1**.

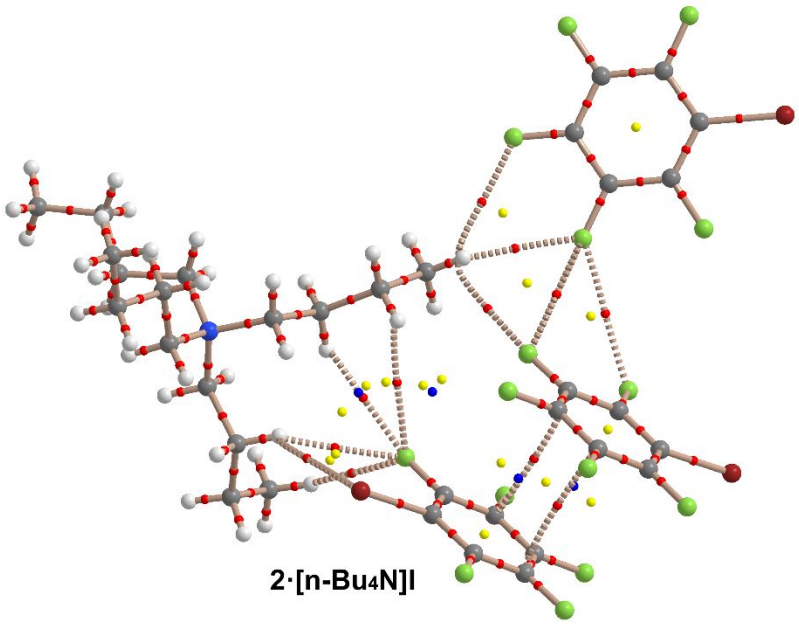

Fig. S4. Distribution of bond, ring and cage critical points (red, yellow and blue spheres, respectively) and bond paths for the adduct **2**·[n-Bu_4N]I at the PBE1PBE-D3/def2-TZVP level of theory.

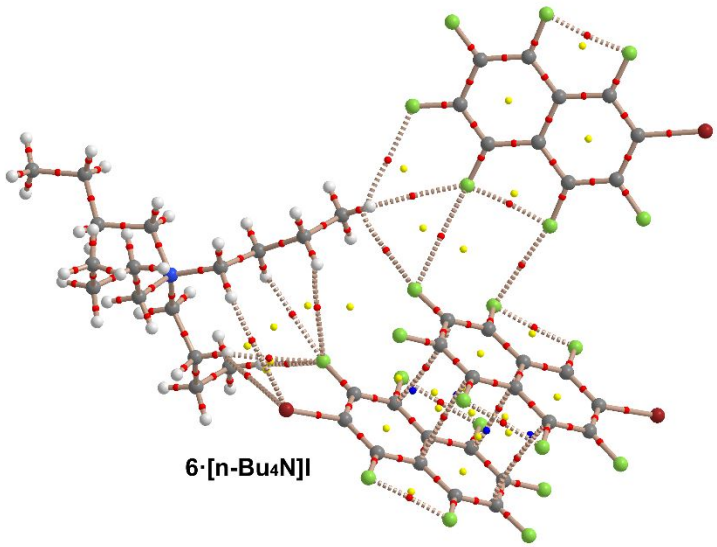

Fig. S5. Distribution of bond, ring and cage critical points (red, yellow and blue spheres, respectively) and bond paths for the adduct **6**·[n-Bu_4N]I at the PBE1PBE-D3/def2-TZVP level of theory

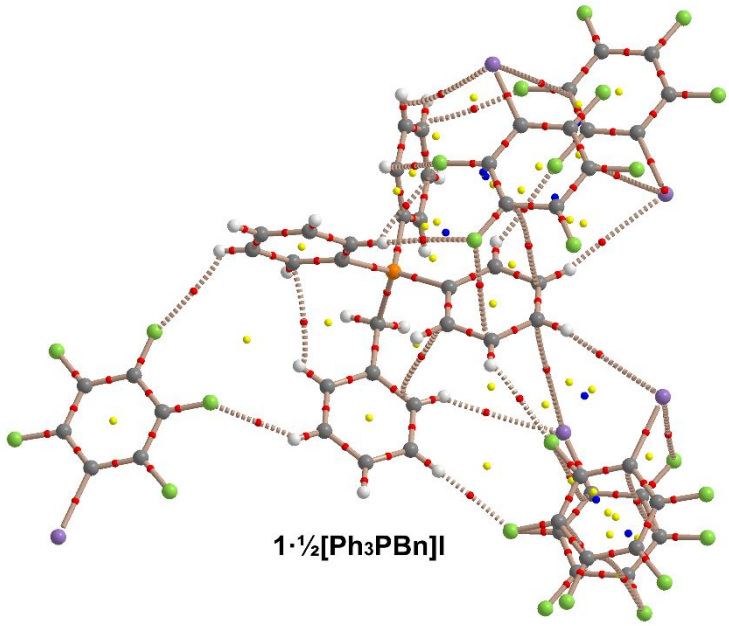

Fig. S6. Distribution of bond, ring and cage critical points (red, yellow and blue spheres, respectively) and bond paths for the adduct **1**·½[Ph_3NBn]I at the PBE1PBE-D3/def2-TZVP level of theory

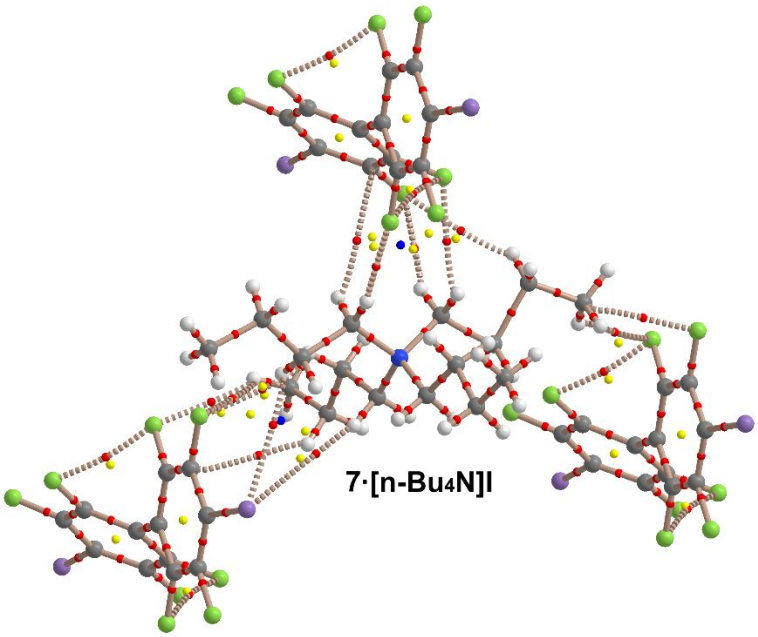

Fig. S7. Distribution of bond, ring and cage critical points (red, yellow and blue spheres, respectively) and bond paths for the adduct **7**·[n-Bu_4N]I at the PBE1PBE-D3/def2-TZVP level of theory

Table S6. Results of the Hirshfeld surface analysis for the XRD structures of the obtained adducts.

XRD structure	Contributions of different intermolecular contacts to the molecular Hirshfeld surface*
1·½[Ph_3PBn]I	H–F 33.5%, F–F 14.6%, C–F 13.3%, H–I 12.4%, C–C 9.0%, I–F 8.2%, C–I 4.5%, I–I 3.0%, H–C 1.4%
2·[*n*-Bu_4N]I	H–F 34.5%, F–F 24.3%, H–Br 16.9%, C–F 9.3%, H–C 6.9%, C–C 5.1%, I–Br 2.0%, Br–F 1.0%
3·[*n*-Bu_4N]I	F–F 33.0%, H–F 22.8%, C–F 22.2%, H–I 13.0%, H–C 4.3%, C–C 2.8%, I–I 1.6%
6·[*n*-Bu_4N]I	H–F 27.6%, F–F 26.8%, C–F 16.7%, H–Br 13.2%, C–C 7.9%, H–C 5.7%, I–Br 1.6%
7·[*n*-Bu_4N]I	H–F 45.1%, H–I 17.8%, H–C 13.7%, I–F 6.8%, C–I 6.0%, F–F 5.2%, I–I 3.5%, C–F 2.0%

*The contributions of all other intermolecular contacts do not exceed 1

$^{13}C\{^{19}F\}$ and ^{19}F spectra of synthesized compounds.

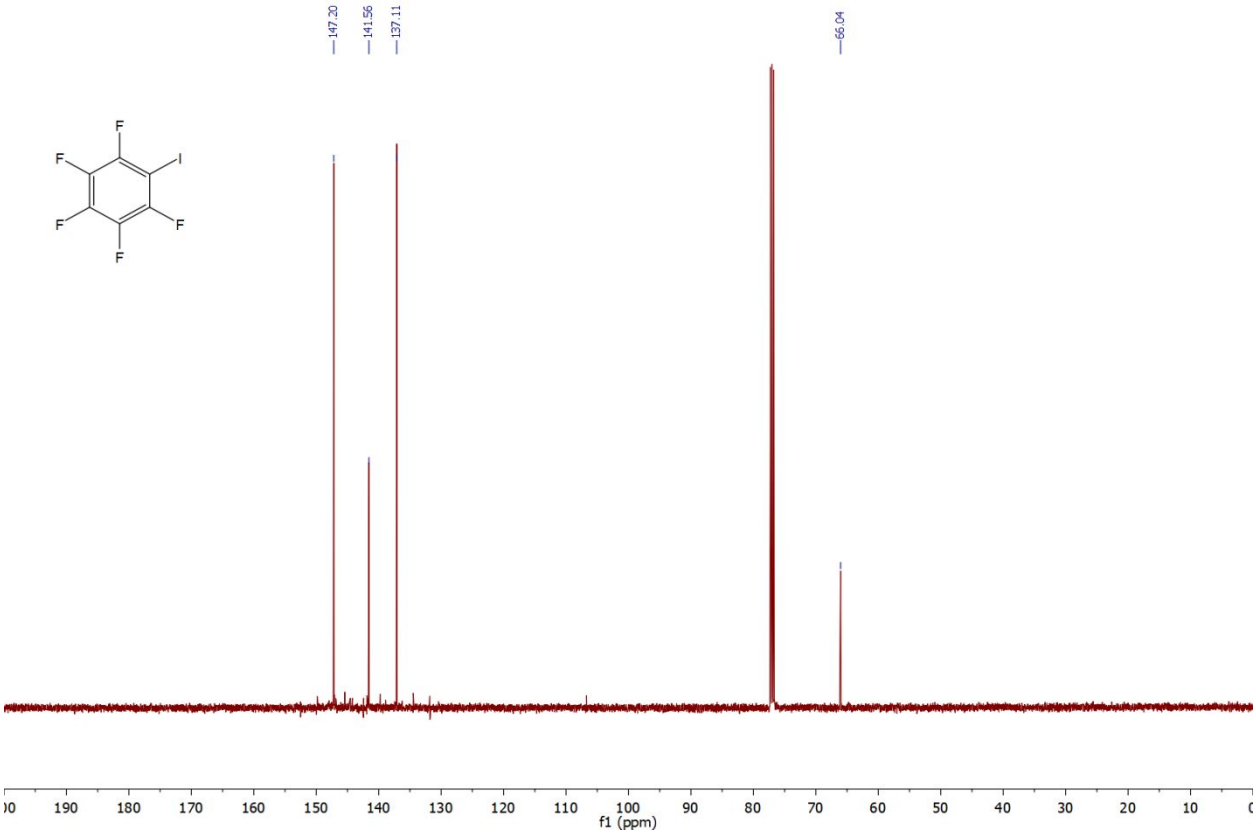

Fig. S8. $^{13}C\{^{19}F\}$ spectrum of **1.**

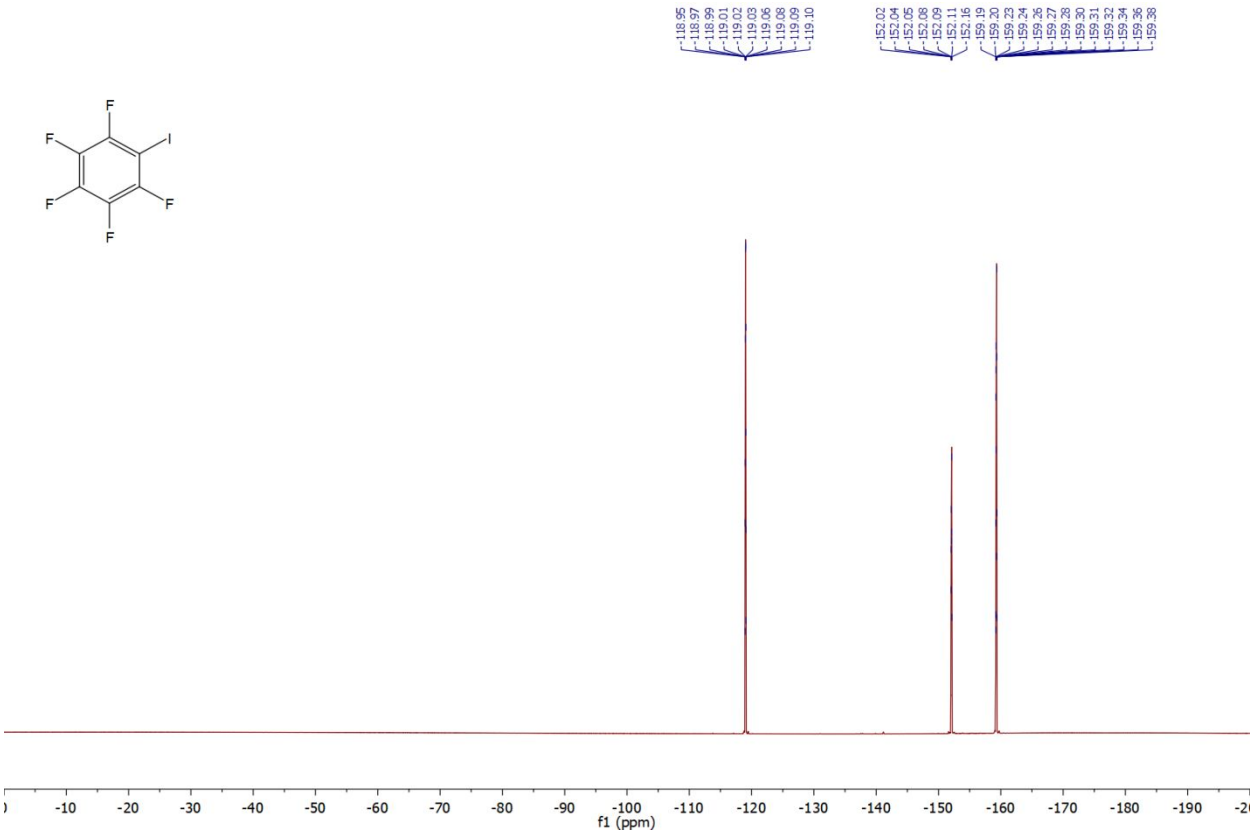

Fig. S9. ^{19}F spectrum of **1.**

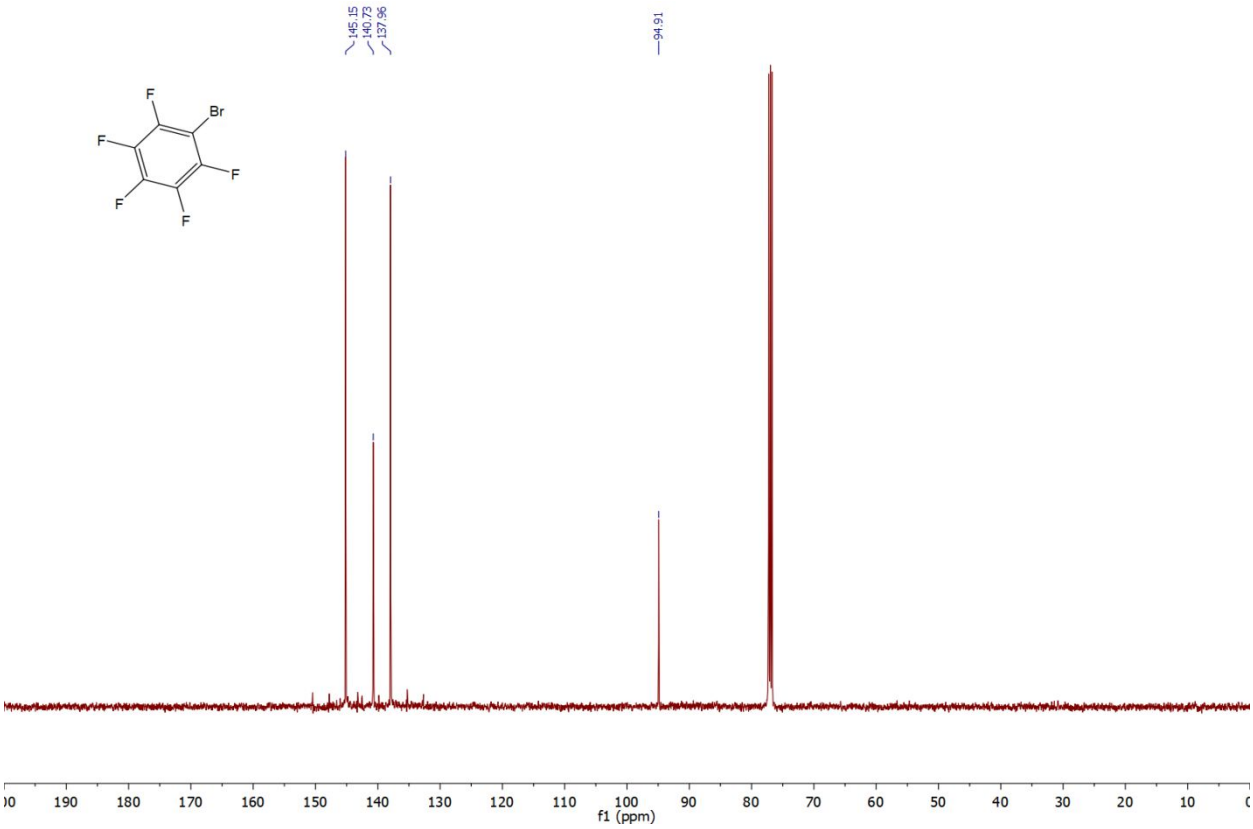

Fig. S10. $^{13}C\{^{19}F\}$ spectrum of **2.**

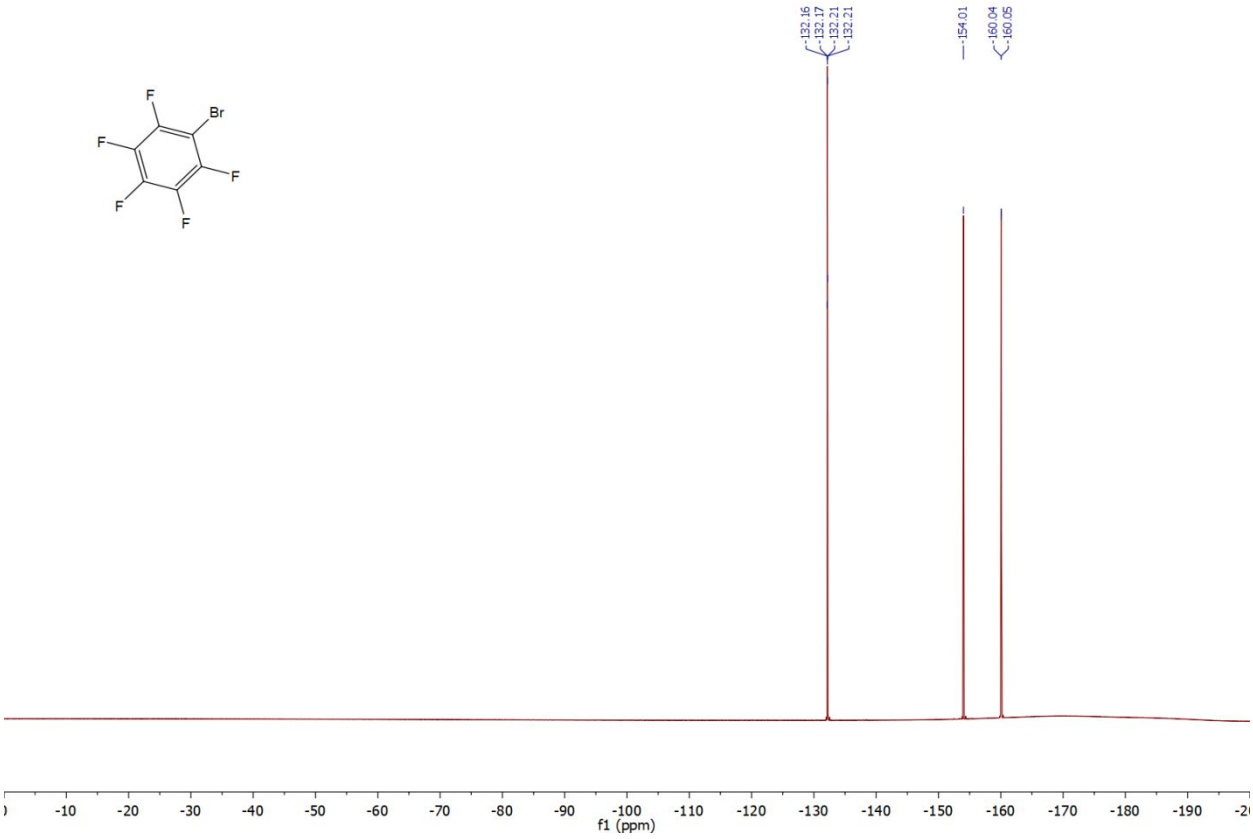

Fig. S11. ^{19}F spectrum of **2.**

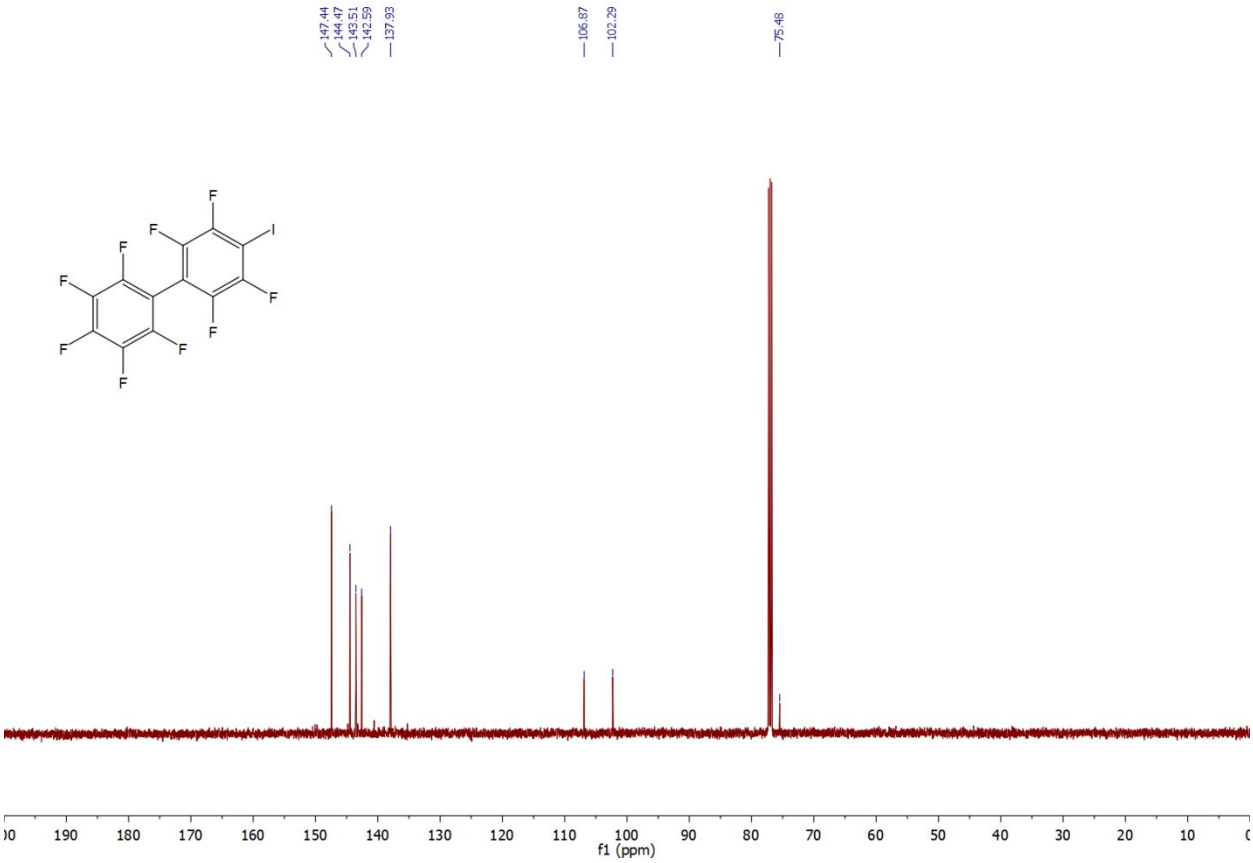

Fig. S12. $^{13}C\{^{19}F\}$ spectrum of **3.**

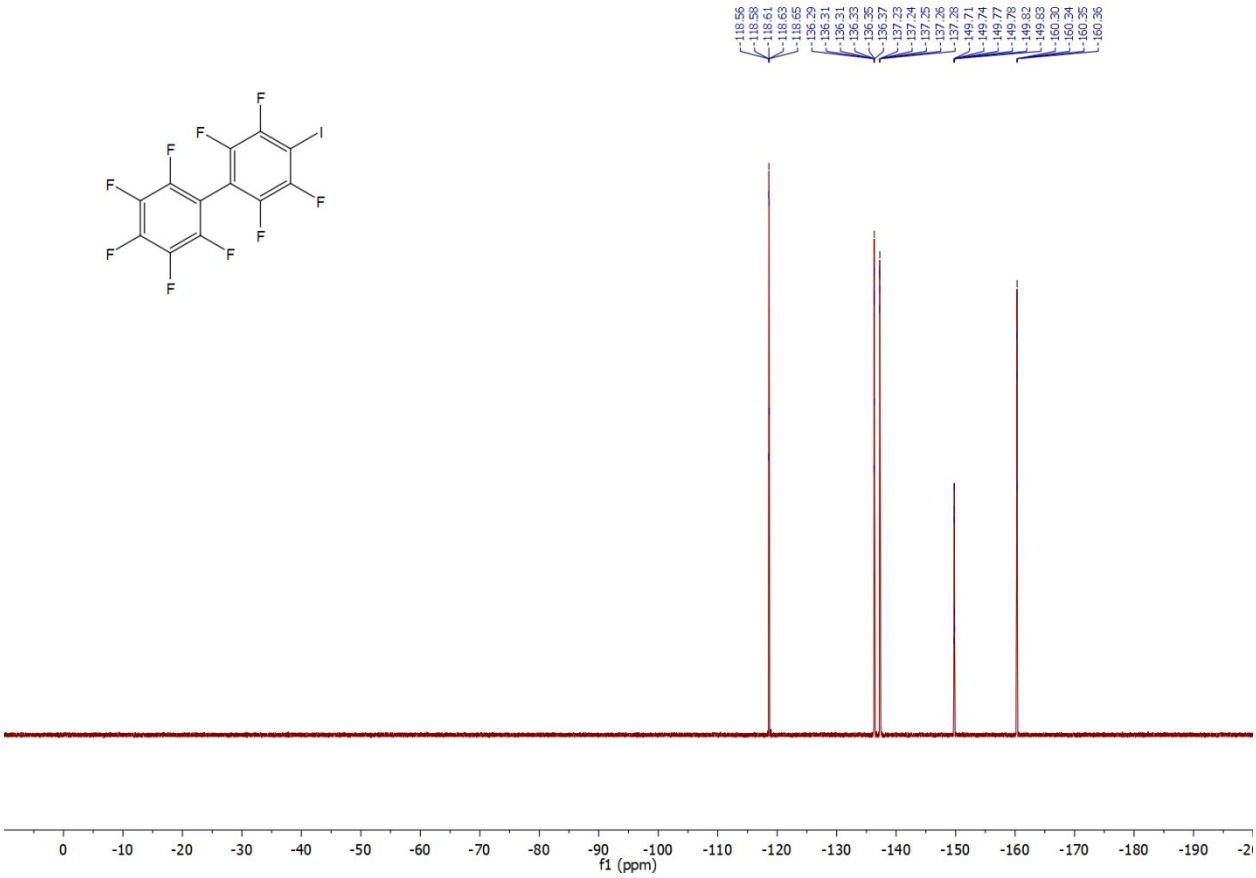

Fig. S13. ^{19}F spectrum of **3.**

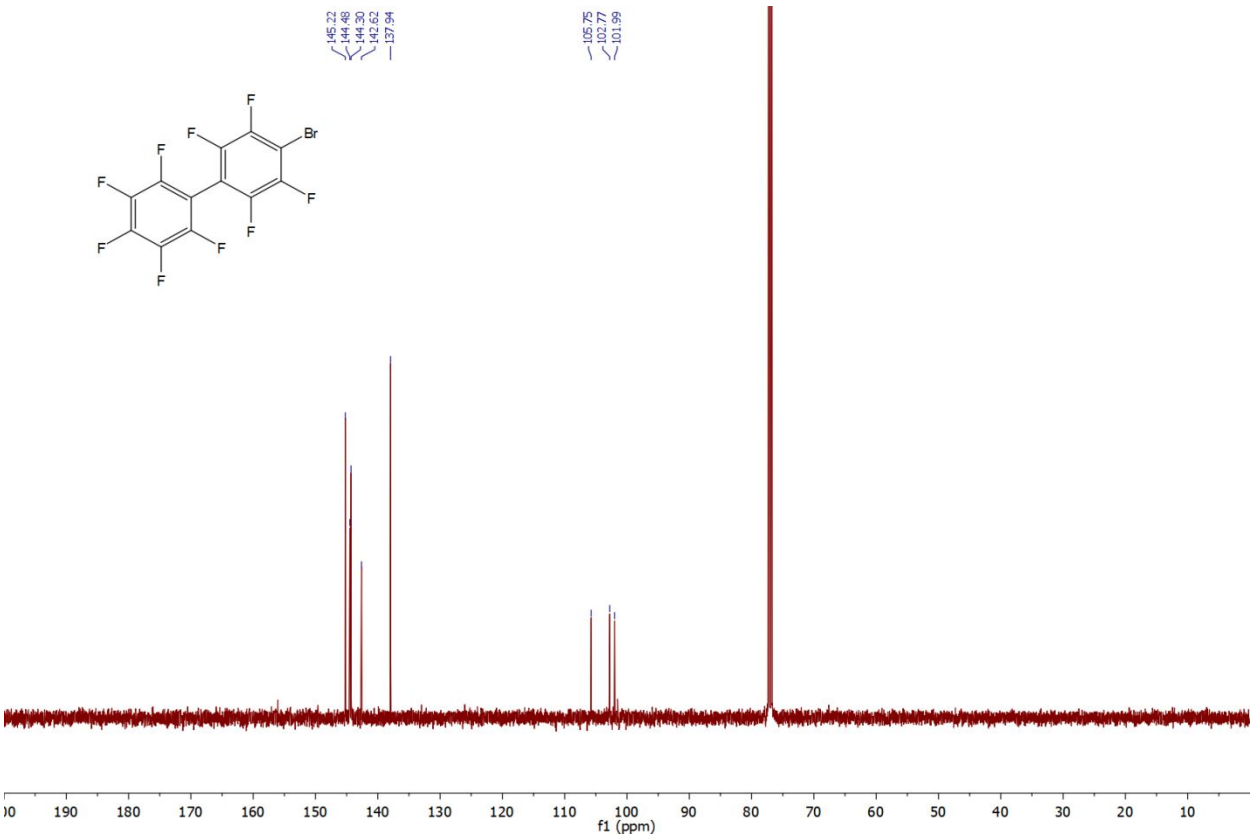

Fig. S14. $^{13}C\{^{19}F\}$ spectrum of **4.**

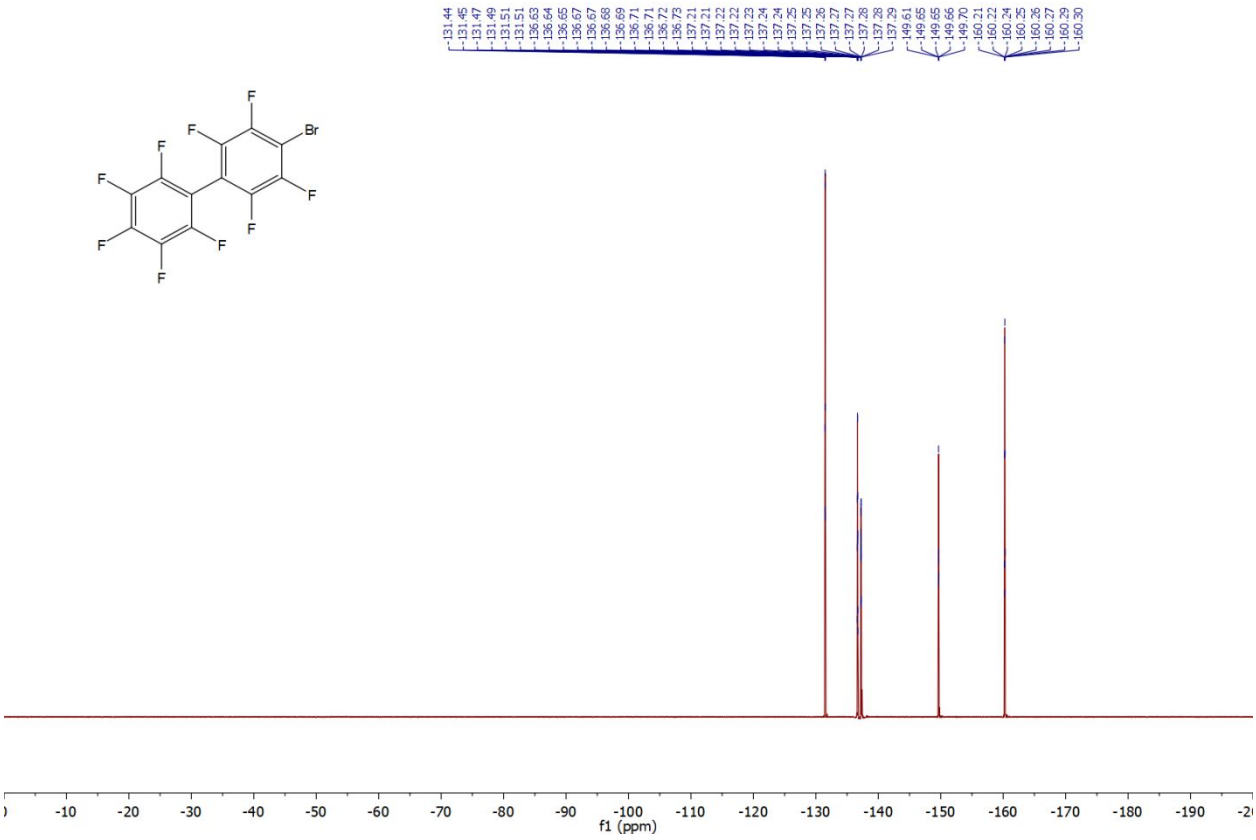

Fig. S15. ^{19}F spectrum of **4.**

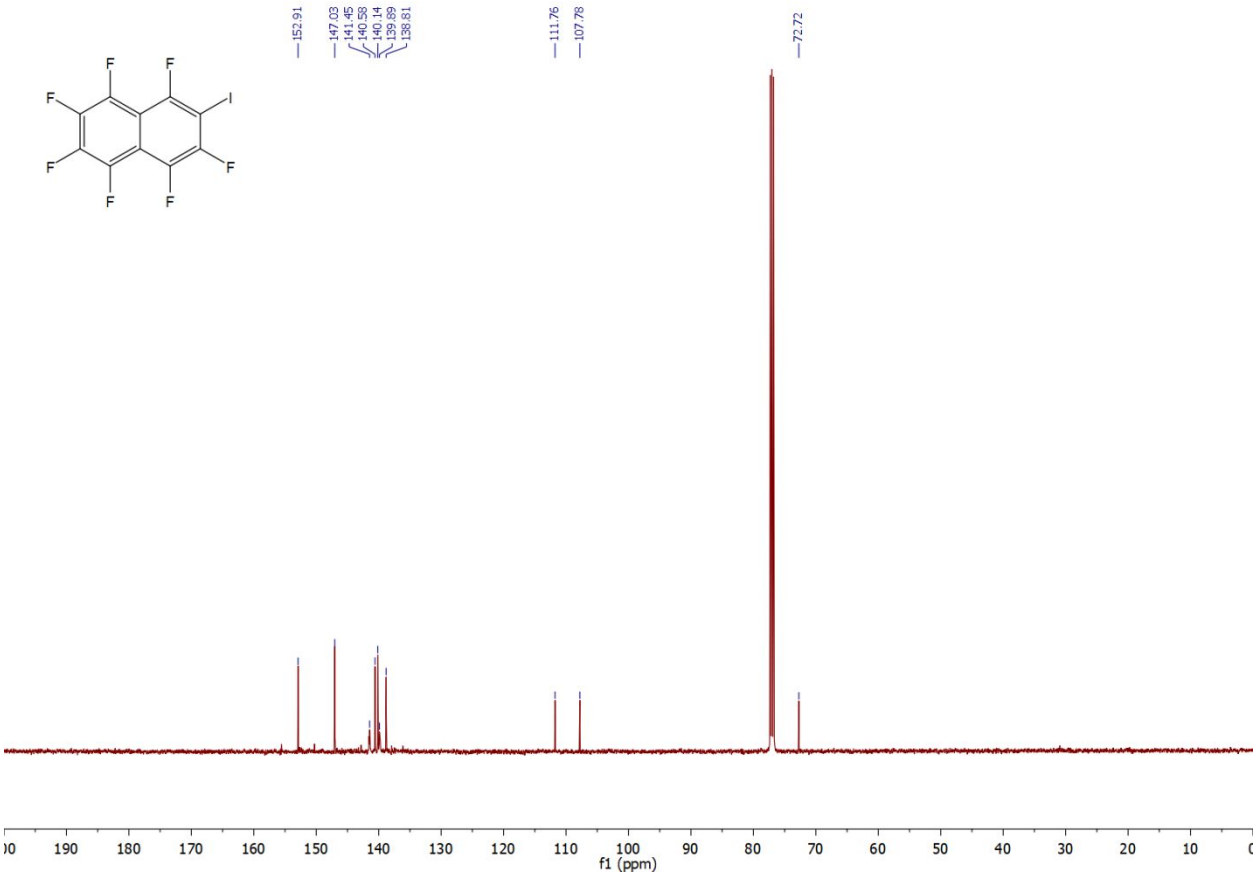

Fig. S16. $^{13}C\{^{19}F\}$ spectrum of **5.**

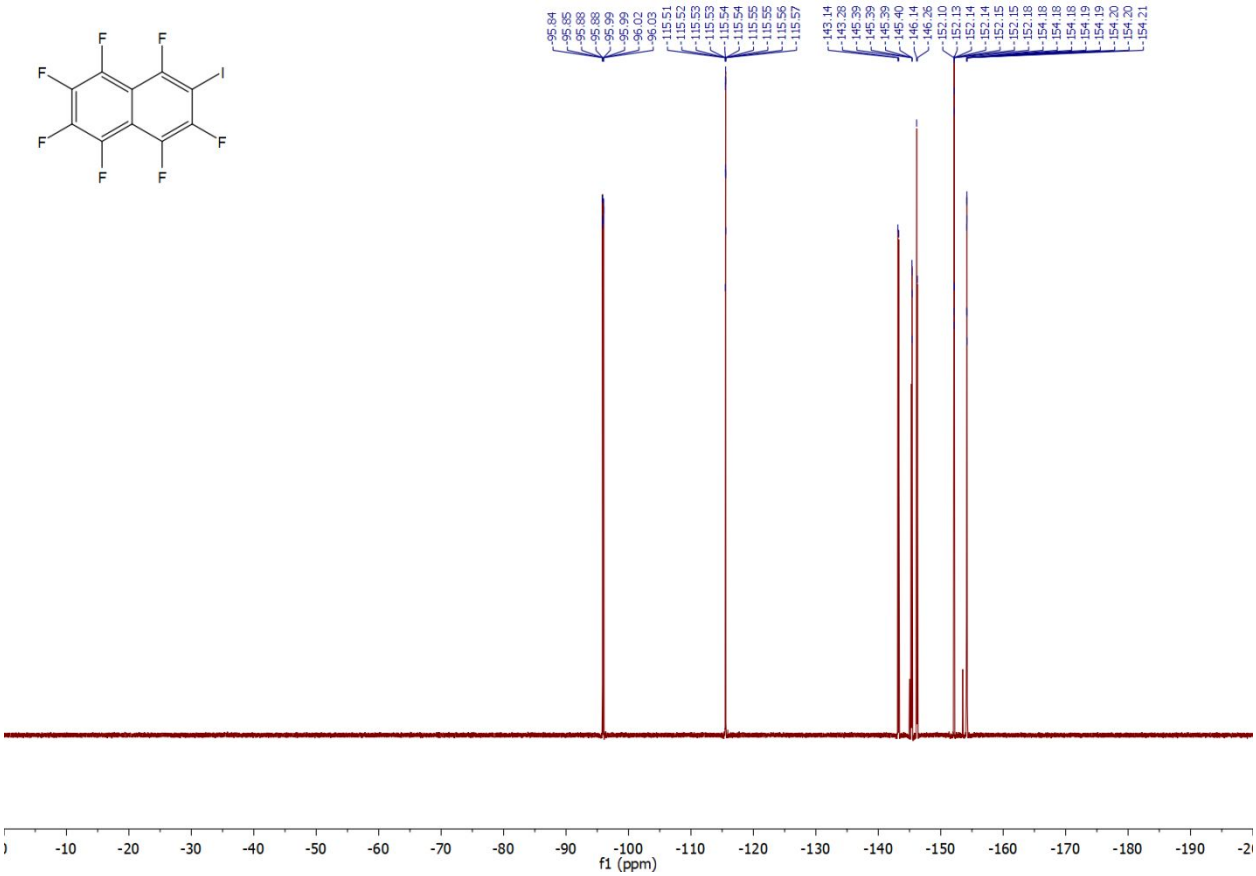

Fig. S17. ^{19}F spectrum of **5.**

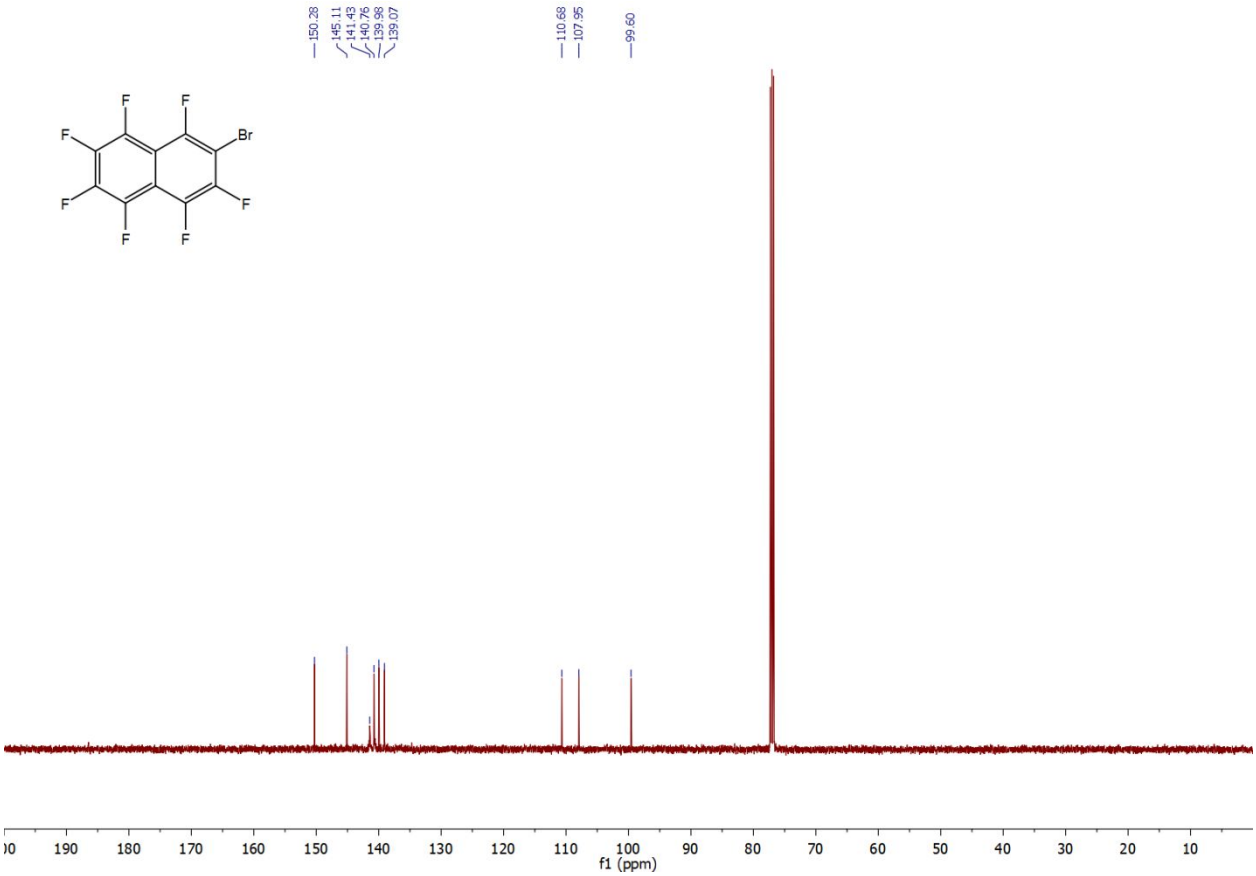

Fig. S18. $^{13}C\{^{19}F\}$ spectrum of **6.**

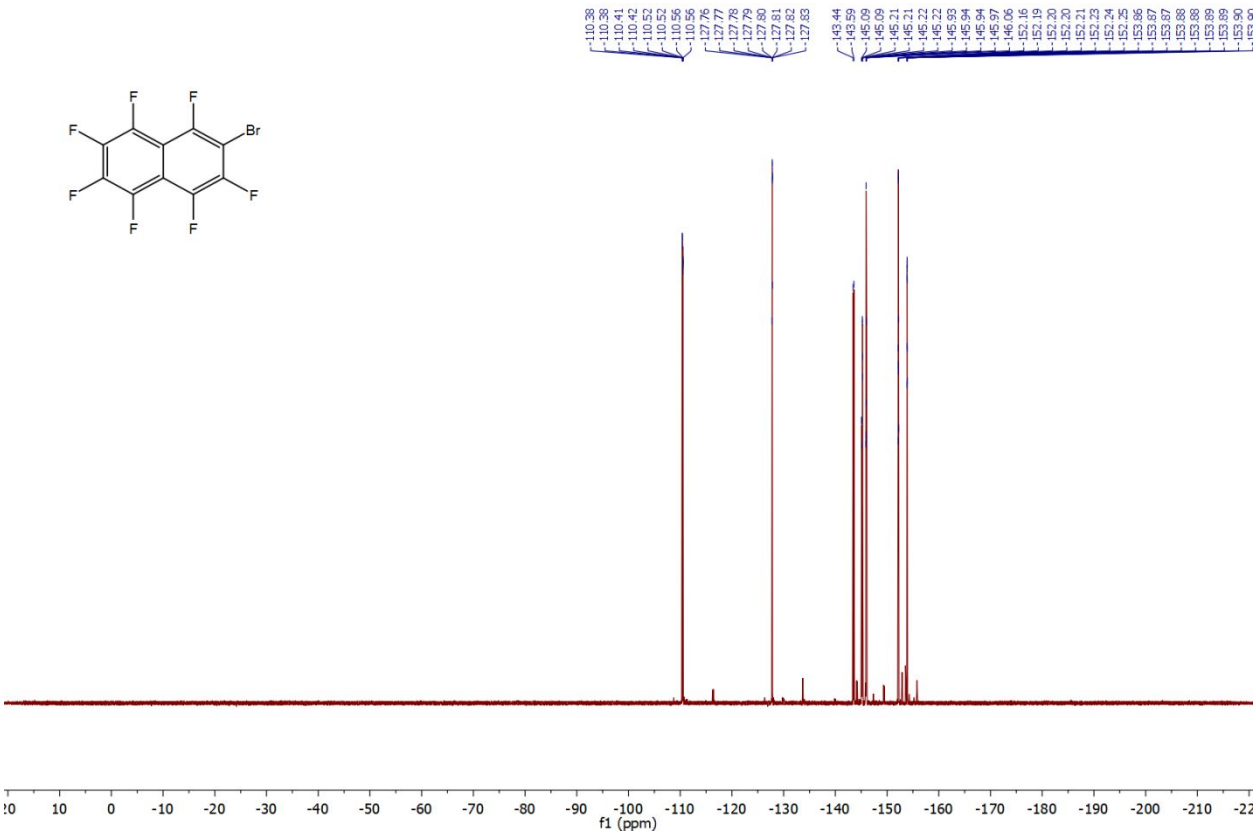

Fig. S19. ^{19}F spectrum of **6.**

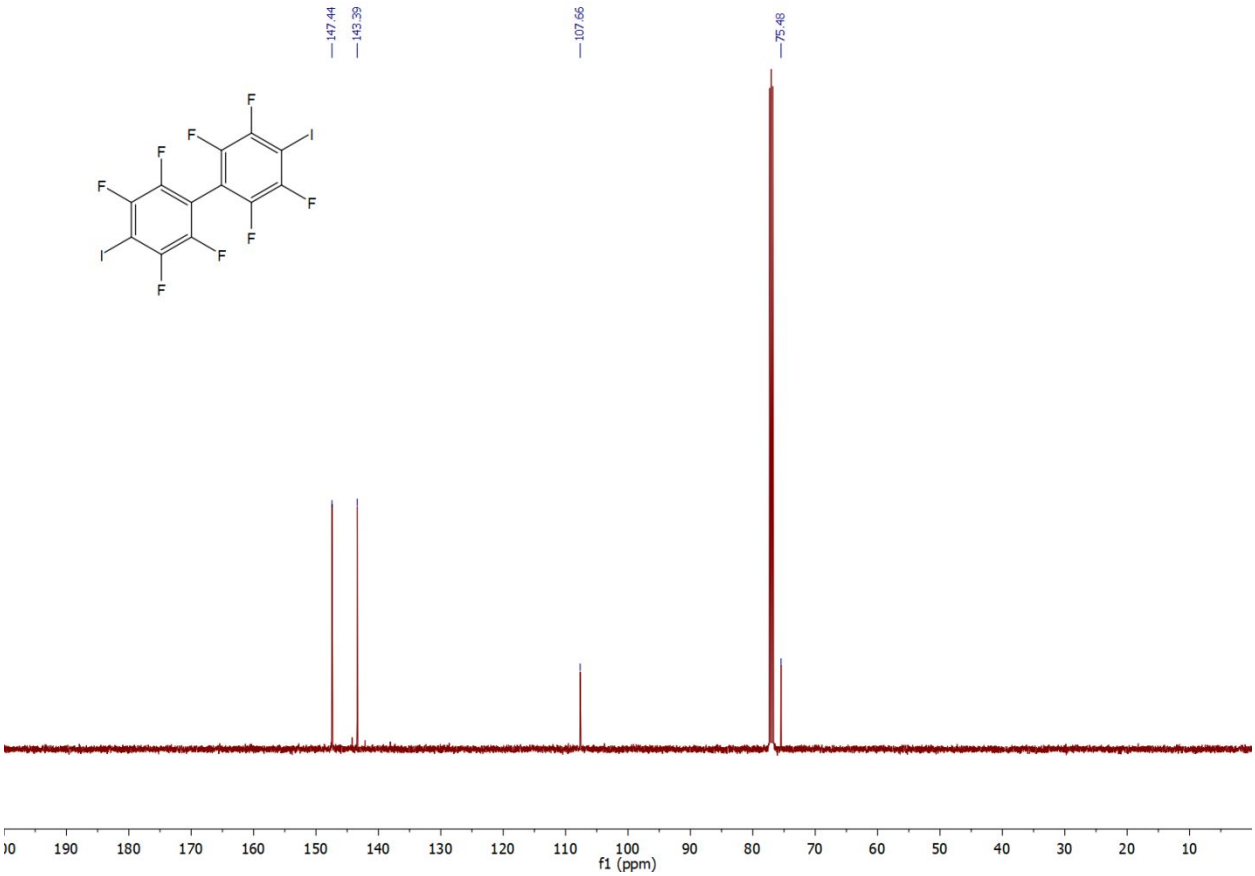

Fig. S20. $^{13}C\{^{19}F\}$ spectrum of **7.**

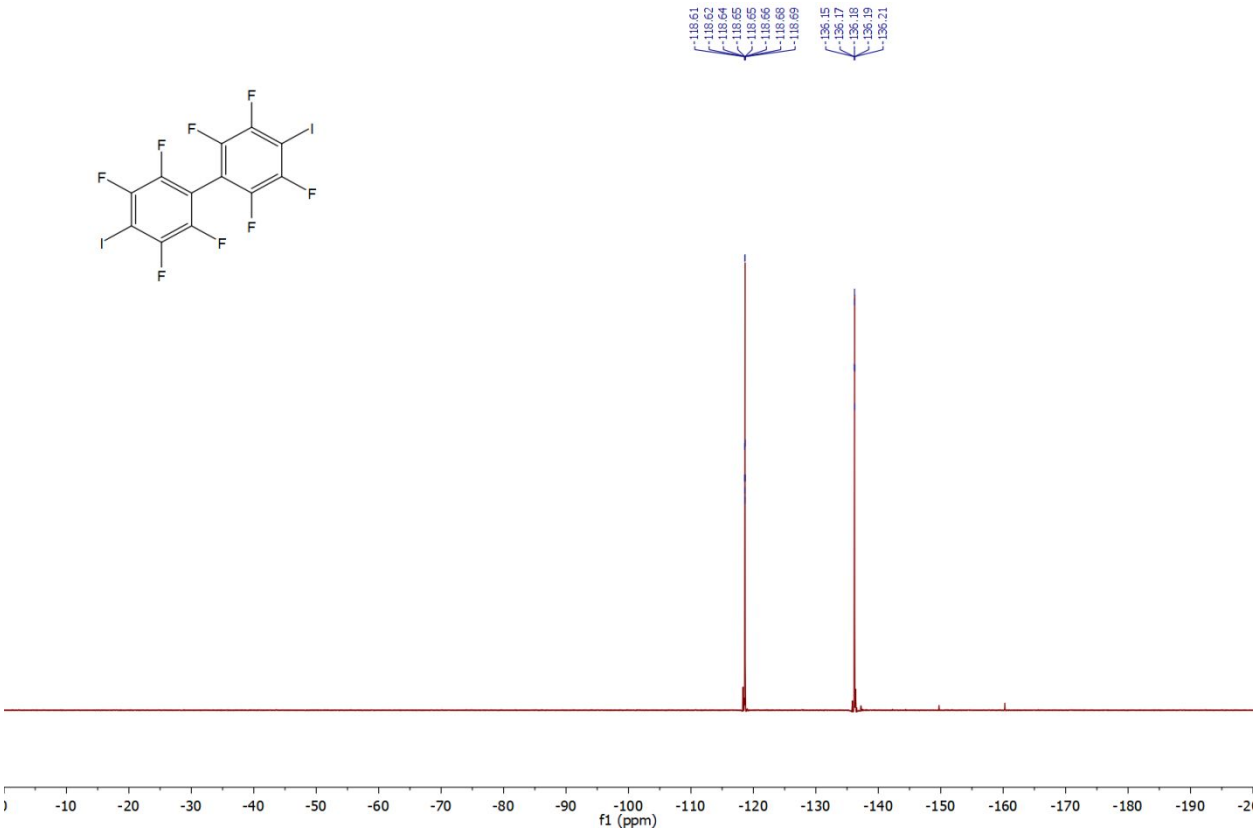

Fig. S21. ^{19}F spectrum of **7.**

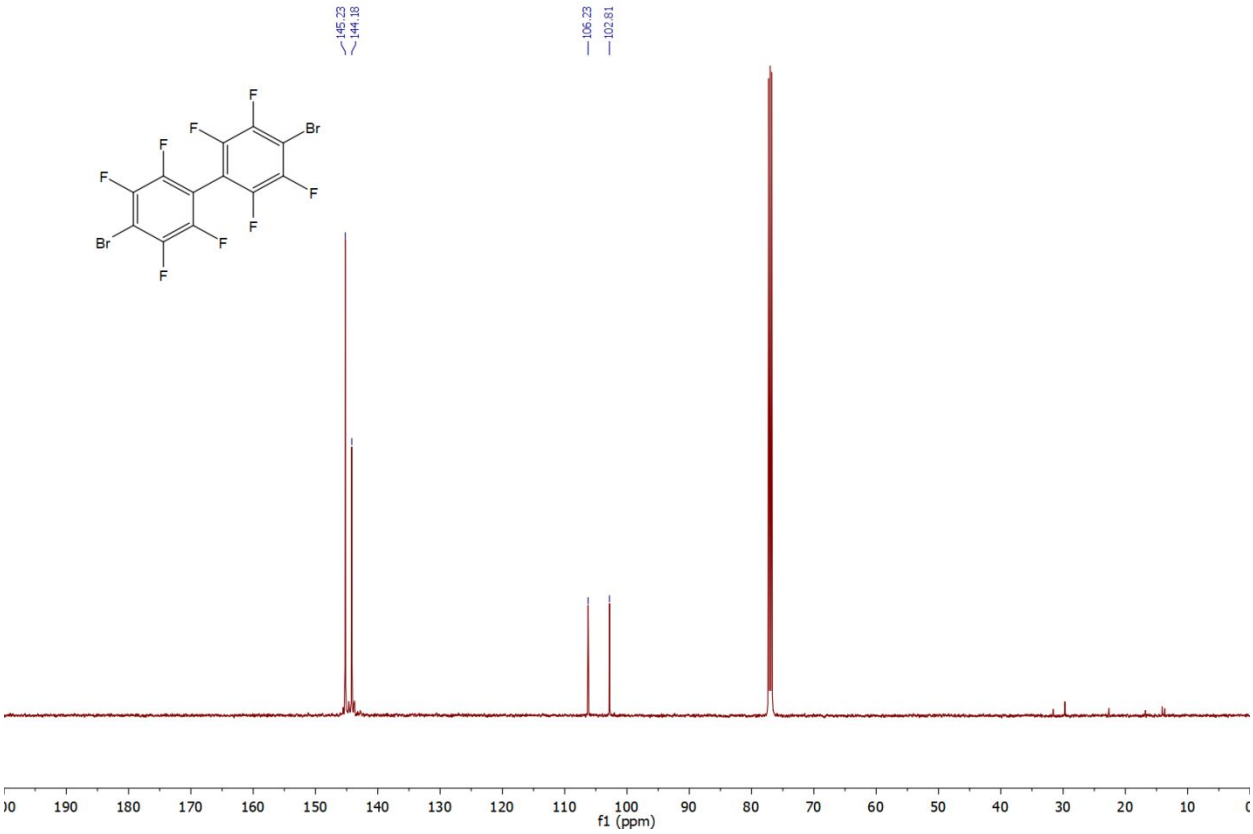

Fig. S22. $^{13}C\{^{19}F\}$ spectrum of **8.**

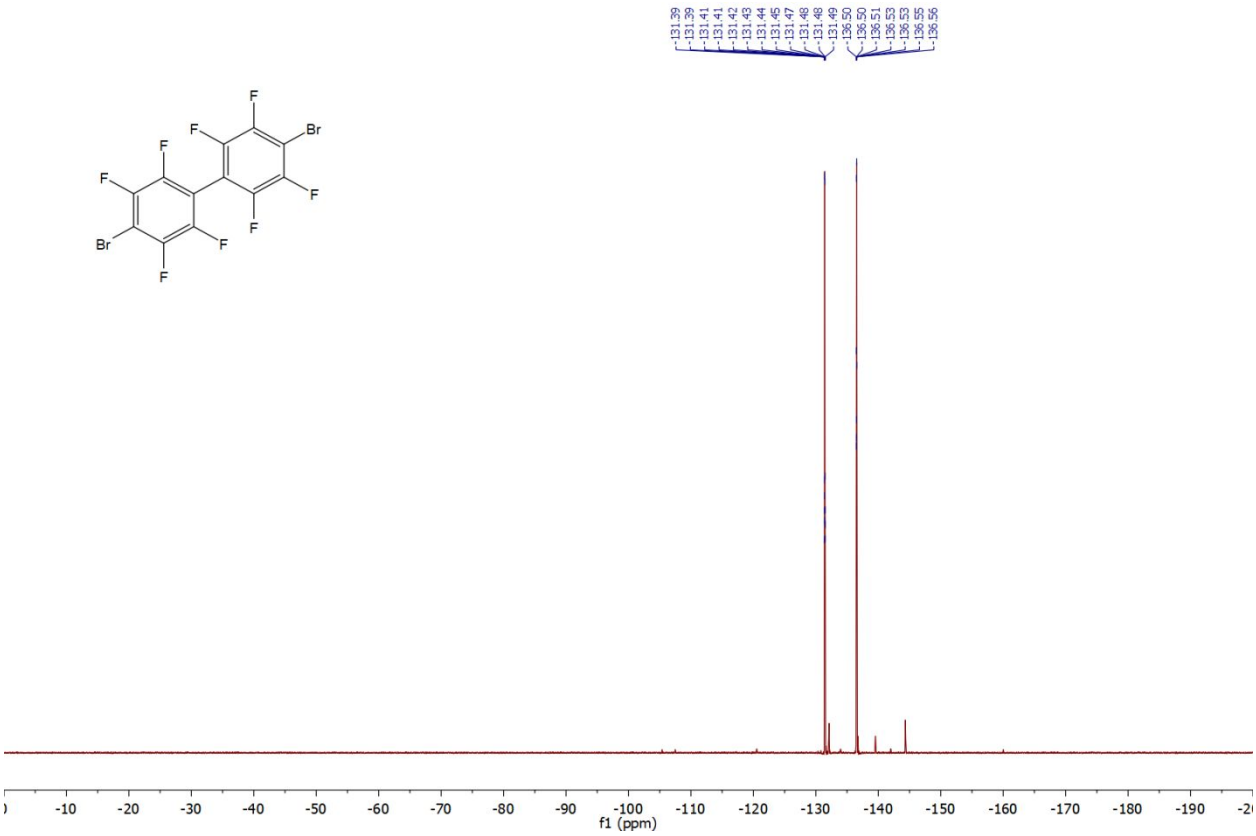

Fig. S23. ^{19}F spectrum of **8.**